



Strong double space-time wave packets using optical parametric amplification

Zhaoyang Li ^{1,2}✉, Yuxin Leng² & Ruxin Li ^{1,2,3}

The space-time (ST) wave packet, a type of light source with many anomalous behaviors, has already found application in weak-field optics, however its generation method limits its energy and therefore its application in strong-field optics. Here we show that the type-I collinear optical parametric amplification (OPA) is a natural amplifier for a ST wave packet, because in it, the ST spectrum (i.e., angle-dependent phase-matching spectrum) of the signal and idler has the same analytical expression as that of a ST wave packet under the narrowband approximation. The high gain in a thin-crystal OPA allows for large energy amplification while ensuring unchanged ST correlation. Meanwhile, a double ST wave packet containing two collinear-propagating ones of the amplified signal and the generated idler via the nondegenerate OPA is reported, which with short- and long-wavelengths (relative to the degenerate-wavelength) have superluminal and subluminal velocities, respectively. This study realizes energy amplification, wavelength conversion, and velocity switching of a ST wave packet and will expand its application in many fields.

¹Zhangjiang Laboratory, Pudong, Shanghai 201210, China. ²Shanghai Institute of Optics and Fine Mechanics, Chinese Academy of Sciences, Jiading, Shanghai 201800, China. ³ShanghaiTech University, Pudong, Shanghai 201210, China. ✉email: lizy@zjlab.ac.cn

The spatiotemporal coupling, as an ever-changing optics tool, recently has been well studied to realize kinds of light sources for optical and physical applications^{1–10}. Two recent representative examples are “flying focus” proposed by Sainte-Marie et al. and Froula et al.^{11,12} and “ST wave packet” proposed by H.E. Kondakci and A.F. Abouraddy^{13,14}, which are special sets of spatiotemporal structured pulses¹⁵ and can propagate at any velocity, i.e., higher or lower than the light speed and forward or backward along the optical axis. The former has already been applied for overcoming dephasing in laser wakefield accelerators¹⁶, producing arbitrary velocity ionization waves¹⁷, etc. in strong-field optics, and the latter also has great potentials from optical imaging, microscopy, communication to micro-particle manipulation. Apart from wide-range tunable velocities and accelerations^{18–21}, the ST wave packet has many other features, including diffraction-free²², tunable dispersion^{23,24}, anomalous refraction²⁵, anomalous ST dispersion effect²⁶, veiled Talbot effect²⁷, time diffraction²⁸, etc., which would be certainly as important as “flying focus” in the strong-field optics. However, producing a ST wave packet needs to accurately control its ST spectrum in the Fourier space to introduce a necessary ST correlation that is transverse spatial-frequency dependent quasi-monochromatic spectral-frequency^{29–31}, and in this process, a phase spatial light modulator (SLM) or phase plate is required at the Fourier plane of a grating 4-*f* setup^{14,32}. The low damage threshold of SLM or phase plate determines that the ST wave packet generator cannot operate at a high energy level, and the same problem also occurs with other spatiotemporal optical fields generated by metasurfaces^{33–35}. Consequently, an efficient amplifier is required, but which must keep the ST correlation unchanged. Because of a low gain (e.g., $\sim 3 \times$ per 7 mm in a conductive-cooled Yb:YAG³⁶), the high-energy amplification of a population inversion amplifier with an energy-level laser medium requires a long-length propagation and/or a multiple-pass configuration, which consequently is not suitable here. OPA based on the three-wave coupling in a nonlinear crystal can realize a high gain within a thin crystal (e.g., $20 \times$ per 0.5 mm in a 40 fs type-I-BBO OPA³⁷ and $10^6 \times$ per 15 mm in a 3 ps type-I-BBO OPA³⁸), which might be an ideal amplifier for a ST wave packet. Previously, the phase matching of some localized waves, such as

focused wave modes, X-waves, O-waves, etc., in nonlinear crystals has been studied, and the generation/amplification of the above localized waves in the optical parametric process has been investigated^{39–43}. Recently, nonlinear effects of newly reported spatiotemporal pulsed beams with orbital angular momentum, optical vortices, arbitrary vectors, etc. also have been demonstrated^{44–46}. All these works show that it is possible to amplify a ST wave packet in OPA.

In this article, we report, under the narrowband approximation, the ST spectrum (angle-dependent phase-matching spectrum) of the type-I collinear OPA has the same analytical expression with that of a ST wave packet, which accordingly is a natural amplifier for a ST wave packet. The amplified signal keeps the ST correlation of the incident ST wave packet, and the simultaneously generated idler also has a high ST correlation which therefore is another ST wave packet, forming a collinear-propagating double ST wave packet. In the non-degenerate OPA, two ST wave packets within the double ST wave packet at short- and long-wavelengths (relative to the degenerate-wavelength) have superluminal and subluminal velocities, respectively; and in the degenerate OPA, it becomes a luminal quasi-monochromatic (the degenerate-wavelength) plane-wave pulse. Our numerical simulation has verified the theoretical prediction and could also be applied in experiments.

Results

ST spectra of ST wave packet and OPA. Figure 1a shows in the Fourier space (momentum space) k_x - k_z - k that corresponds to the physical space (position space) x - z - t , where x and z are the transverse and longitudinal space axes and t is the time axis, the ST spectrum of a ST wave packet lies in the intersecting curve between the light-cone and a spectral plane parallel to the k_x -axis^{13,14,18–31}, and satisfies

$$\cos \Delta\theta = \frac{\omega_0 + \Omega \cot \alpha}{\omega_0 + \Omega}. \quad (1)$$

ω_0 is the vertex frequency defined as the intersecting point between the ST spectrum and the plane $k_x = 0$ at the direction

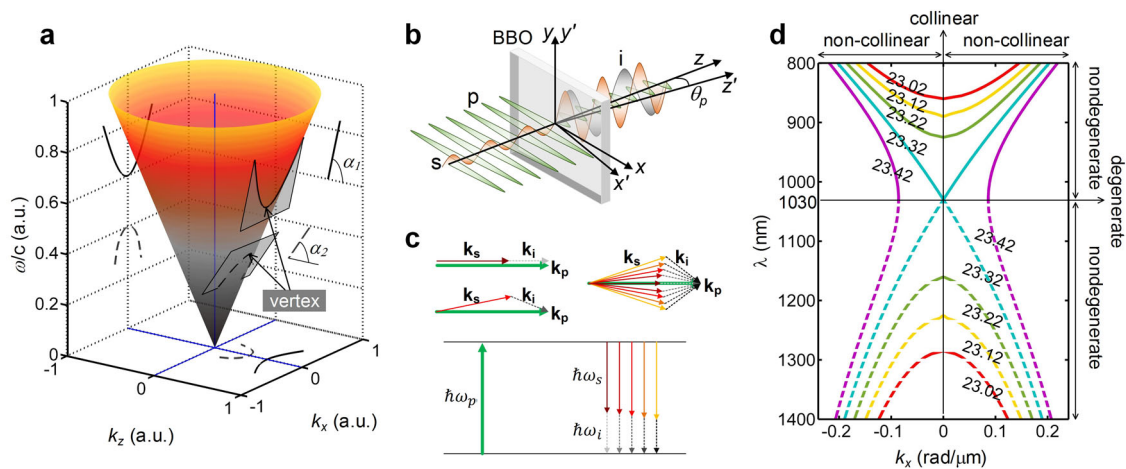


Fig. 1 Space-time (ST) spectra of space-time wave packet and optical parametric amplification (OPA). **a** ST spectrum of a ST wave packet lies in the intersecting curve between the light-cone and a tilted spectral plane parallel to the k_x -axis (here two ST wave packets with spectral plane tilt angles $\alpha_1 > 45^\circ$ and $\alpha_2 < 45^\circ$). Color of the light-cone schematically illustrates the frequency. **b** Three-wave coupling in the type-I OPA (here BBO). x - y - z and x' - y' - z' are lab and crystal coordinates. θ_p is the pump angle with respect to the z' -axis. p , pump; s , signal; and i , idler. **c** Phase-matching (momentum conservation) and energy conservation diagrams for collinear OPA, non-collinear OPA, and ST wave packet OPA. Different colors of the arrows schematically illustrate different frequencies. **d** Phase-matching curves in a 515 nm pumped type-I BBO crystal when the pump angle θ_p varies from 23.02° to 23.42° every 0.1° (distinguished by colors). Degenerate, nondegenerate, collinear, and non-collinear zones are given. When a signal/idler lies in the solid line and at one side of $k_x = 0$, its idler/signal lies in the dash line and at the other side of $k_x = 0$.

$k_z > 0$, its direction is the propagating direction of the ST wave packet, and its coordinates are $(k_x, k_z, \omega/c) = (0, k_0, \omega_0/c)$. $\Omega = \omega - \omega_0$ is the frequency difference about ω_0 of each spectral component, and $\Delta\theta$ is its propagating angle with respect to the direction of ω_0 (or the ST wave packet) which is spectral-dependent. α is the tilt angle of the spectral plane with respect to the k_z -axis, which determines the velocity of a ST wave packet $v_g/c = \tan\alpha$ ^{19,29}. Figure 1a illustrates a superluminal and a subluminal ST wave packets with $\alpha_1 > 45^\circ$ and $\alpha_2 < 45^\circ$ at high and low vertex frequencies ω_0 , respectively.

Figure 1b shows in the type-I (o + o → e) collinear OPA, three waves propagate along the z -axis, and the energy is transferred from the strong pump (e-light) to the amplified signal (o-light) and the generated idler (o-light) in a thin nonlinear crystal (BBO here). We define x - y - z and x' - y' - z' are the lab and crystal coordinates, respectively; θ_s, θ_p and θ_i are propagating angles of the signal, idler and pump in the x' - y' - z' plane of the crystal coordinates x' - y' - z' ; and, because the pump always propagates at the z -axis in the lab coordinates x - y - z , $\Delta\theta_s = \theta_s - \theta_p$ and $\Delta\theta_i = \theta_i - \theta_p$ are propagating angles of the signal and idler in the lab coordinates x - y - z . The relative rotation angle θ_p between the x - y - z and x' - y' - z' coordinates about the y/y' -axis changes the refractive index of the pump (e-light) in the crystal for phase-matching. Traditional collinear and non-collinear phase-matchings (momentum conservation) and energy conservation are illustrated in Fig. 1c. If a ST wave packet can satisfy the amplification condition, Fig. 1c shows the pump spectrum, signal spectral components and idler spectral components should firstly satisfy energy conversion $\omega_s + \omega_i = \omega_p$ and secondly contain a collinear phase-matching $k_{s0} + k_{i0} = k_p$ for the vertex frequency ω_0 of the signal and a series of spatially symmetric non-collinear phase-matchings $k_s \cos\Delta\theta_s + k_i \cos\Delta\theta_i = k_p$ for other frequencies $\omega = \omega_0 + \Omega$ of the signal. And then, the pump beam and the signal and idler ST wave packets approximately form a collinear OPA. Although different spectral components of the signal and the idler have different but spatially symmetric propagating directions, the two propagation-invariant wave packets both propagate at the z -axis. Using a 515 nm pump, phase-matching curves for different pump angles θ_p from 23.02° to 23.42° every 0.1° are calculated and shown in Fig. 1d. Here, we use solid and dash curves denote the signal and idler, respectively, which are defined relative to each other and are interchangeable. The pump is always along $k_x = 0$, for the collinear phase-matching, both the signal and idler are along $k_x = 0$; and for non-collinear phase-matchings, the signal and idler are at either side of the pump. Comparing the angle-dependent phase-matching spectrum (here also named as ST spectrum) of the signal or idler (see Fig. 1d) with the ST spectrum of a ST wave packet (see Fig. 1a), they have quite similar profiles in the λ - k_x (or ω/c - k_x) plane, i.e., continuous symmetric conic curves about $k_x = 0$. If two curves overlap with each other, all spectral components including the vertex frequency ω_0 and the other frequencies $\omega = \omega_0 + \Omega$ of a ST wave packet would be simultaneously amplified by collinear and non-collinear OPAs, respectively, generating an idler that is also a ST wave packet. The amplified signal and the generated idler would have different frequencies for the non-degenerate OPA and the same vertex frequency for the degenerate OPA, respectively.

To verify this judgment, we derived the analytical expression of the angle-dependent phase-matching spectrum (ST spectrum) of the type-I OPA under the narrowband approximation, which satisfies

$$\cos\Delta\theta_s \approx \frac{\omega_{s0} + \Omega_s(\omega_{s0}n_s^2 + \frac{(\omega_p n_p - \omega_{s0} n_s)^2}{\omega_p - \omega_{s0}})/\omega_p n_p n_s}{\omega_{s0} + \Omega_s}, \quad (2)$$

where, $\Delta\theta_s$ is the propagating angle of the frequency $\omega_s = \omega_{s0} + \Omega_s$ with respect to the vertex frequency ω_{s0} within the signal ST wave packet in the x - y - z coordinates, n_s and n_p are angle-independent and

angle-dependent refractive indices of the signal vertex frequency ω_{s0} (o-light) and the pump frequency ω_p (e-light), respectively, and a constant n_s is used for all frequencies of the signal under the narrowband approximation. By comparing Eq. (2) with (1), the ST spectrum (angle-dependent phase-matching spectrum) of the signal in the type-I OPA has the same expression with that of a ST wave packet, which indicates that a ST wave packet can be amplified by a matched type-I OPA.

Velocities of amplified and generated ST wave packets. From Eqs. (1) and (2), the requirement of amplifying a ST wave packet by a matched OPA is the tilt angle α_s of the spectral plane forming the ST wave packet in the Fourier space needs to satisfy

$$\cot\alpha_s \approx \frac{\omega_{s0}n_s^2 + \frac{(\omega_p n_p - \omega_{s0} n_s)^2}{\omega_p - \omega_{s0}}}{\omega_p n_p n_s}. \quad (3)$$

The refractive indices n_s and n_p in the crystal can be calculated by the Sellmeier equation for ω_{s0} and ω_p , respectively, and the pump angle θ_p is contained in n_p . Because three-wave coupling equations show the signal and idler are interchangeable in mathematics [see Eq. (5) in “Methods”], the generated idler is another ST wave packet, whose ST spectrum $\Delta\theta_i(\Omega_i)$ and spectral plane tilt angle α_i are also respectively described by Eqs. (2) and (3) by simply replacing the subscript s by i . After OPA, a double ST wave packet would appear which contains the amplified signal as well as the generated idler.

When solving the collinear phase-matching [Eq. (5) in “Methods”] in a 515 nm pumped type-I BBO crystal, for every pump angle θ_p in the phase-matching region, two phase-matched vertex wavelengths λ_0 of the signal and idler in a double ST wave packet can be calculated, and by substituting into Eq. (3), their velocities can be obtained ($v_g/c = \tan\alpha$). Figure 2 shows the relationship among the pump angle, the vertex wavelength of the signal/idler and the velocity of the ST wave packet, and a signal/idler and its idler/signal lie in red and black curves, respectively. When the pump angle is $\theta_p < 23.32^\circ$ or $\theta_p = 23.32^\circ$, OPA is nondegenerate or degenerate, respectively, and the double ST wave packet (i.e., signal and idler) has “different wavelengths and velocities” or “same wavelength and velocity”, respectively. In the nondegenerate OPA, the velocities of a double ST wave packet (i.e., signal and idler) are superluminal and subluminal when the vertex wavelengths are shorter and longer than the degenerate-wavelength (1030 nm here), respectively. In this case, the two ST wave packets (i.e., signal and idler) will separate in time during propagation, which can also be separated in spectrum. In the degenerate OPA, the signal and idler have the same vertex wavelength of the degenerate-wavelength (1030 nm here), the same spectral plane tilt angle of 45° in the Fourier space (see Eq. (3)) and accordingly the same velocity of the light speed (as introduced in refs. ^{19,31}), and, in this case, the ST wave packets should become luminal plane-wave pulses. However, Fig. 1d shows because only the vertex wavelength satisfies OPA, other wavelengths cannot be amplified, and the amplified signal and the generated idler would become quasi-monochromatic (the degenerate-wavelength) luminal plane-wave pulses.

Propagation invariance of amplified and generated ST wave packets. In addition to the strict phase-matching ($\Delta k = 0$), small phase-mismatches ($\Delta k \rightarrow 0$) can also support OPAs, and Fig. 3a, b show the gain spectra in a 2 mm thin type-I BBO crystal when the pump wavelength, angle, and intensity are 515 nm, $\theta_p = 23^\circ$, and 10 GW cm^{-2} , respectively. Although two gain spectra in both short- and long-wave ranges have some ST correlations (see Fig. 3a, b), Fig. 3e, f show the supported pulsed beams have Gaussian ST

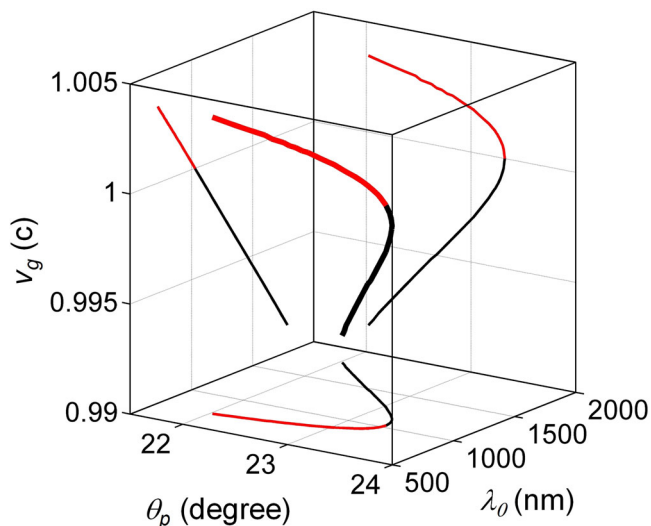


Fig. 2 Relationship between vertex wavelength and velocity of space-time (ST) wave packet with pump angle of collinear optical parametric amplification. When the collinear phase-matching is satisfied (515 nm pumped type-I BBO crystal here), each pump angle θ_p corresponds to two (vertex) wavelengths λ_0 (red and black), and the (vertex) wavelength λ_0 that is shorter (red) and longer (black) than the degenerate-wavelength (1030 nm here) corresponds to a ST wave packet with a superluminal (red) and a subluminal (black) velocity v_g , respectively.

distributions, which spread out dramatically in space after a 20 mm free propagation (see Fig. 3i, j). Kondakci et al. have defined a parameter of the correlation uncertainty $\delta\lambda$ between k_x and λ , which is inversely proportional to the propagation-invariant length¹³. Large correlation uncertainties $\delta\lambda = 43$ and 99 nm at the short- and long-wave gain spectra in Fig. 3a, b destroy high ST correlations, and therefore it is not easy to generate long-distance diffraction-free beams directly in optical parametric generation (OPG), optical parametric oscillation (OPO), etc. However, seeding OPA with a localized wave packet can suppress the optical parametric fluorescence/generation, whose ST correlation is determined by the incident signal instead of OPA, and thereby it may be a good solution. A seed ST wave packet is produced using Eq. (3), whose parameters include a reduced correlation uncertainty $\delta\lambda = 2$ nm, a vertex wavelength $\lambda_0 = 855$ nm, a spectral bandwidth $\Delta\lambda = 40$ nm, and a spectral plane tilt angle in the Fourier space $\alpha = 45.0572^\circ$. The ST spectra of the amplified signal and the generated idler are illustrated in Fig. 3c, d, the parameters of the signal almost remain unchanged, and those of the idler include a correlation uncertainty $\delta\lambda = 4.7$ nm, a vertex wavelength $\lambda_0 = 1295$ nm, a spectral bandwidth $\Delta\lambda = 105$ nm, and a spectral plane tilt angle in the Fourier space $\alpha = 44.9111^\circ$. The 10 GW cm⁻² strong pump enables 400 × small-signal gain for the signal and idler of the same energy level. Figure 3g, h show the pulsed beams supported by the ST spectra of the signal and idler, respectively, and both have a typical distribution of a ST wave packet with a butterfly-like shape and a central peak^{13,14}. Although the “central peaks” are enlarged in space and time (compare Fig. 3g, h and e, f), which almost do not spread out after a 20 mm long-distance free propagation much exceeding the Rayleigh length (see Fig. 3k, l). We can also find some small mis-matches between the ST spectra of the signal and idler ST wave packets with the strict phase-matching curves (green dash lines in Fig. 3a–d), especially when the wavelengths are far away from the vertex wavelengths, which is because the narrowband approximation for Eq. (2) cannot be strictly satisfied for a broadband pulsed beam. However, the ST spectra of the signal and idler ST wave packets still lie in the gain spectral ranges of OPA [compare Fig. 3c, d and a, b], which therefore

doesn't obviously affect amplification. Figure 4a, b respectively show the ST spectra of the incident and the amplified signal ST wave packets, and the mis-matching reduces the relative intensity at the short-wavelength of the amplified signal (compare parts in the blue rectangles in Fig. 4b with those in Fig. 4a). Figure 4c, d give the local-time integral intensity distributions $I(x, z)$ during a 100 mm long-distance free propagation of the incident and the amplified signal ST wave packets, respectively, and no difference can be observed. In experiments, the perfect phase-matching (amplification condition) can be obtained by reducing both the spectral bandwidth $\Delta\lambda$ and the correlation uncertainty $\delta\lambda$ of the signal ST wave packet, and in refs. 14,19 which are only $\Delta\lambda = 0.92$ nm & $\delta\lambda = 30$ pm and $\Delta\lambda = 0.3$ nm & $\delta\lambda = 24$ pm, respectively, and much (~50–100 times) smaller than the value $\Delta\lambda = 40$ nm & $\delta\lambda = 2$ nm in this article. Figure 3c also shows when $\Delta\lambda < 10$ nm, the narrowband approximation would work very well.

Propagation of double ST wave packet. The free propagation of the amplified signal and the generated idler in vacuum are simulated and shown in Fig. 5. OPA happens at the position $z = 0$, where the signal and idler overlap in space and time. After $z = 0$, the separation between two ST wave packets increases with propagation due to different velocities of the signal and idler $v_{gs} = 1.0020c$ and $v_{gi} = 0.9969c$. Figure 5 also shows the propagation-invariant length of the idler is shorter than that of the signal. The first reason is the Rayleigh length for a fixed beam waist w_0 decreases with increasing the wavelength (e.g., Gaussian beam $Z_R = \pi w_0^2/\lambda$). Here, both central-peak waists of the signal and idler ST wave packets are around $w_0 = 23.5$ μm, however due to a longer wavelength (1295 and 855 nm vertex wavelengths for the idler and signal), the Rayleigh length of the idler $Z_{Ri} = 1.3$ mm is shorter than that of the signal $Z_{Rs} = 2.0$ mm. The second reason is the correlation uncertainty of the idler $\delta\lambda = 4.7$ is larger than that of the signal $\delta\lambda = 2$ and accordingly shortens the propagation-invariant length. Even so, Fig. 5 shows both the propagation-invariant lengths of the signal and idler have far exceeded their Rayleigh lengths of $Z_{Rs} = 2.0$ mm and $Z_{Ri} = 1.3$ mm, respectively.

Discussion

In this article, a general concept of amplifying a ST wave packet in the type-I OPA is studied, and a plane-wave quasi-monochromatic (515 nm) pump pulsed beam without any temporal and spatial phase distortion is considered. However, when the pump pulse has a temporal phase distortion, it will transmit to the amplified signal and the generated idler pulses. In addition, the propagation in the nonlinear crystal can also introduce some temporal dispersions. A current study shows a weak temporal phase distortion cannot affect the propagation invariance of a ST wave packet obviously⁴⁷. Similarly, when the pump beam has a spatial phase distortion, it will also transmit to the amplified signal and the generated idler beams. Because the beam aperture of a ST wave packet usually is very small (here ~30 μm), the wavefront error of the pump beam within such a narrow size is negligible. Here, the OPA works at a small-signal gain level, and when at a saturation gain level, the amplified signal and the generated idler pulsed beams will contain nonlinear temporal and spatial phase distortions. In general, the amount is very small and therefore does not affect the propagation invariance of the ST wave packet, either. In future, these engineering factors need to be studied in the next-step research for kinds of application. The result in this article is based on the type-I phase-matching, so not only BBO but also other nonlinear crystals, such as LBO, CLBO, KDP, DKDP, YCOD, etc., are applicable. However, the type-II phase-matching, whose angle-dependent phase-matching

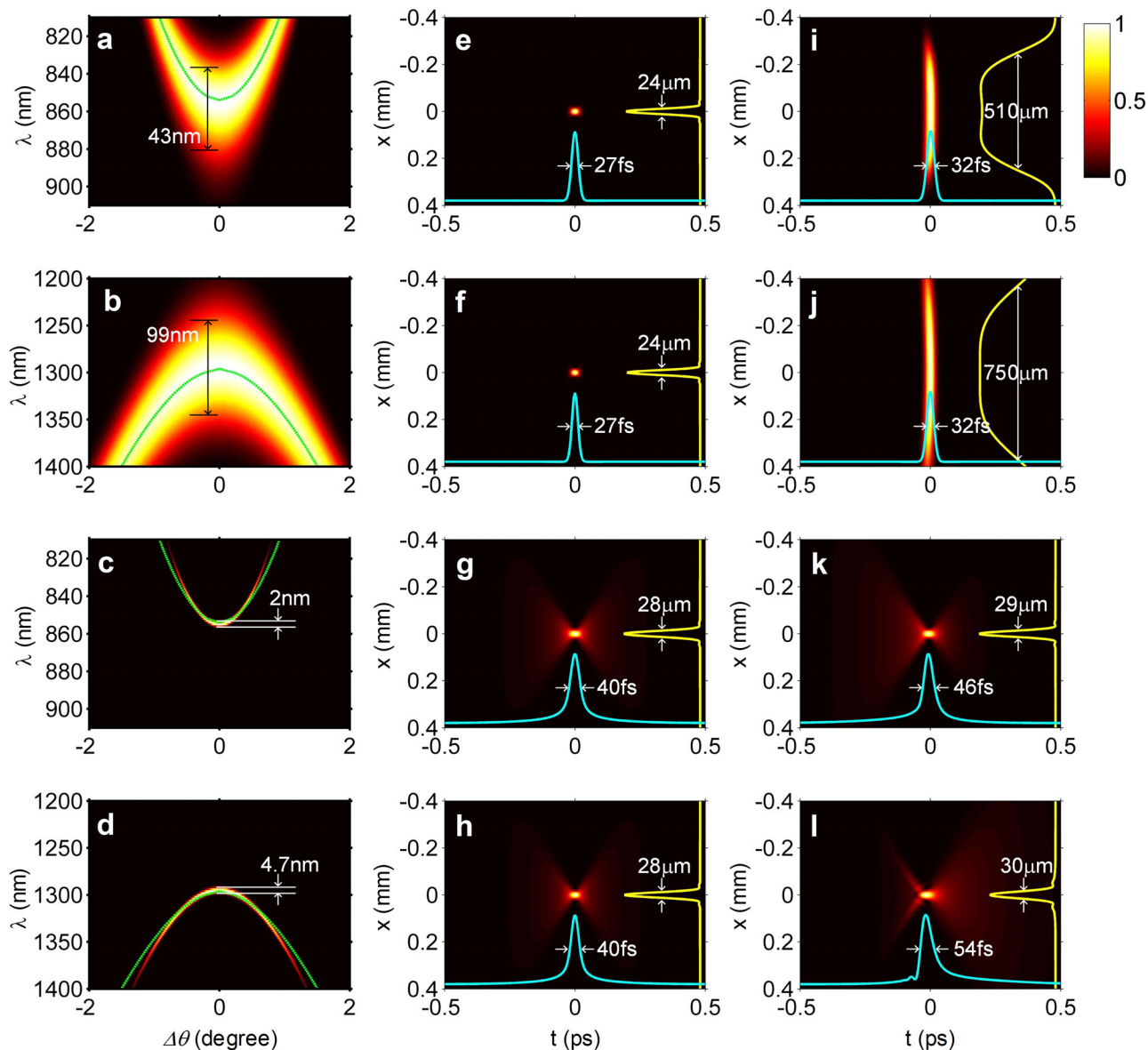


Fig. 3 Space-time (ST) spectra and supported pulsed beams. In a 515 nm pumped type-I BBO crystal with a pump angle $\theta_p = 23^\circ$, gain spectra of optical parametric amplification (OPA)/optical parametric generation (OPG)/optical parametric oscillation (OPO) at **a** short and **b** long wavelengths for different directions. When seeding a ST wave packet, ST spectra of **c** amplified signal and **d** generated idler. Green dash lines in **a-d** are phase-matching curves. $\Delta\theta$ is the angle in the x - z plane with respect to the pump, uncertainties of ST spectra are around 43, 99, 2, and 4.7 nm in (**a-d**). Pulsed beams supported by ST spectra in **a-d** are shown in (**e-h**), and after 20 mm free propagation those are shown in (**i-l**). t is the local time, all figures share a normalized color-bar, and profiles and FWHM (full width at half maximum) widths of on-axis pulses and beams are given by curves in (**e-l**).

spectrum is asymmetric about the pump direction, does not fit the result. Moreover, to amplify all components, the pump pulsed beam should be large enough to completely wrap around the incident signal ST wave packet in space-time (e.g., $> 600 \mu\text{m}$ in space and $> 500 \text{ fs}$ in time in Fig. 3g), and this requirement will reduce the pump-signal conversion efficiency comparing with the traditional OPA, however, which is not a key parameter here.

Conclusions

In summary, we have proposed a principle of amplifying a ST wave packet to high-energy by the type-I collinear OPA, where an idler ST wave packet would be generated simultaneously. Our numerical simulation verified the feasibility of this principle and demonstrated an as yet unreported strong double ST wave packet. In the nondegenerate OPA, two collinear-propagating ST wave

packets at short and long wavelengths (compared with the degenerate-wavelength) are superluminal and subluminal, respectively, which accordingly separate in time during propagation. In the degenerate OPA, the double ST wave packet becomes a quasi-monochromatic (the degenerate-wavelength) luminal plane-wave pulse. Amplifying a ST wave packet in energy will introduce this light source to strong-field optics for studying ST-light-matter interactions. Moreover, the simultaneously generated idler can turn a ST wave packet to another wavelength, such as infrared, visible and ultraviolet wavelengths, and switch the velocity between superluminal and subluminal. This discovery will expand the range of application of the ST wave packet and also have some reference values for the nonlinear amplification and conversion of other spatiotemporal structured lights.

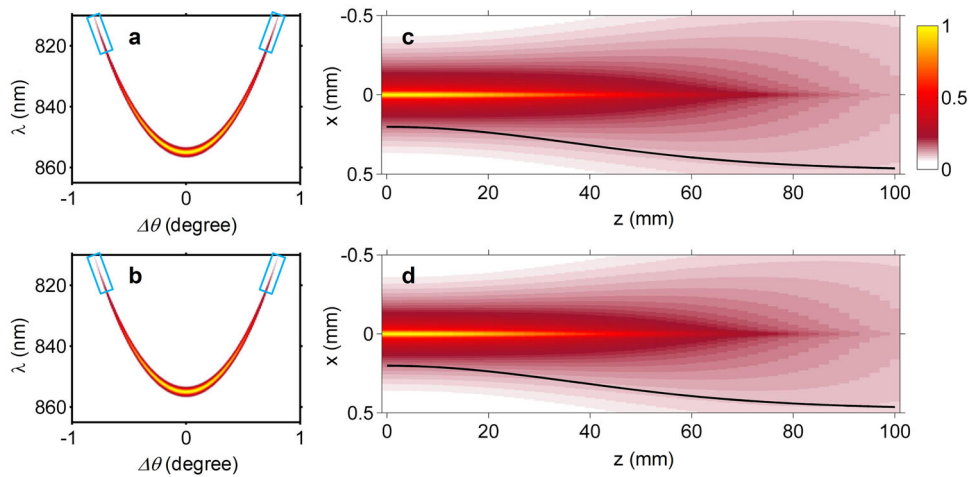


Fig. 4 Comparison between incident and amplified signal space-time (ST) wave packets. ST spectra of **a** incident and **b** amplified signal ST wave packets. Local-time integral intensity distributions during long-distance free propagation $I(x, z)$ of **c** incident and **d** amplified signal ST wave packets. All figures share a normalized color-bar, and black curves in **c** and **d** are on-axis intensities.

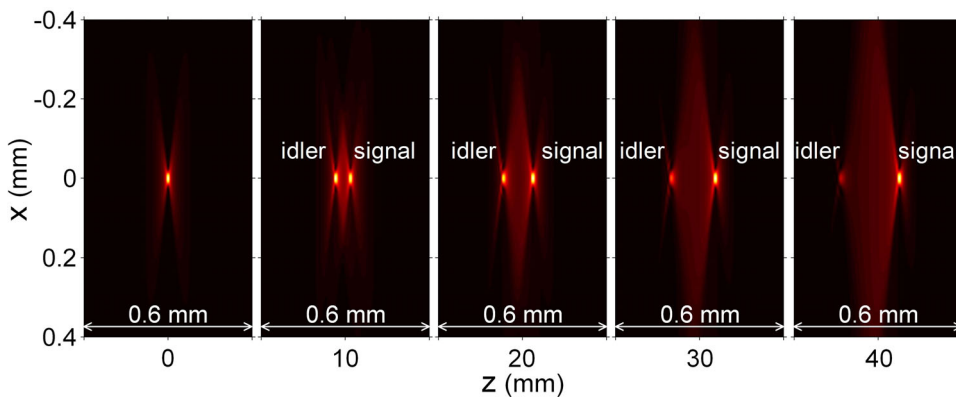


Fig. 5 Double space-time (ST) wave packet propagation in vacuum. Optical parametric amplification (OPA) is at $z = 0$, instantaneous ST distributions at $z = 0, 10, 20, 30,$ and 40 mm, containing two ST wave packets of a superluminal signal and a subluminal idler.

Methods

ST spectrum of ST wave packet. In the Fourier space k_x-k_z-k , the ST spectrum of a ST wave packet is governed by the simultaneous equations of the light-cone and a spectral plane

$$k_x^2 + k_z^2 = k^2, \tag{4a}$$

$$k - k_0 = (k_z - k_0) \tan \alpha, \tag{4b}$$

where, $k = \omega/c$ (in the vacuum) is the wavenumber, $k_x = k \sin \Delta\theta$ and $k_z = k \cos \Delta\theta$ are the transverse and longitudinal components, $\Delta\theta$ is the spectral-dependent propagating angle with respect to that of the vertex frequency, and k_0 is the vertex wavenumber of the ST spectrum defined as the intersecting point between the ST spectrum and the plane $k_x = 0$ at the direction $k_z > 0$ and has the coordinates $(k_x, k_z, k) = (0, k_0, k_0)$. α is the tilt angle of the spectral plane with respect to the k_z -axis. By substituting Eq. (4b) into Eq. (4a) and using $\Omega = \omega - \omega_0$, $|\Delta\theta| < \pi/2$, $|\Omega/\omega_0| < 1$ and $\alpha \sim \pi/4$, we get the ST spectrum of a ST wave packet that is given by Eq. (1) (see equation derivation in Supplementary Note 1 of Supplementary information).

ST spectrum of type-I OPA. The three-wave coupling among the pump, signal and idler satisfies energy conservation and momentum conservation (phase-matching)

$$\omega_s + \omega_i = \omega_p, \tag{5a}$$

$$\mathbf{k}_s + \mathbf{k}_i = \mathbf{k}_p, \tag{5b}$$

where, \mathbf{k} is the wavevector in the nonlinear crystal, and the subscript $s, i,$ and p denotes the signal, idler and pump, respectively. The vertex frequency ω_{s0} of the signal ST wave packet satisfies the collinear phase-matching ($\Delta\theta_{s0} = 0$), and Eq. (5b) becomes $\omega_{s0}n_s + \omega_{i0}n_i = \omega_p n_p$, where ω_{i0} is the idler of ω_{s0} , and $n_s, n_p,$ and n_p are refractive indices of $\omega_{s0}, \omega_{i0},$ and ω_p for the type-I phase-matching. By

substitution of Eq. (5a), n_i is given by

$$n_i = \frac{\omega_p n_p - \omega_{s0} n_s}{\omega_p - \omega_{s0}}. \tag{6}$$

Because the bandwidth of the signal ST wave packet, accordingly that of the generated idler, usually is narrow $|\Omega/\omega_0| \ll 1$, we can approximately use constant refractive indices n_s and n_i for all frequencies of the signal and idler, respectively, which are angle-independent for the type-I phase-matching. Other frequencies $\omega_s = \omega_{s0} + \Omega_s$ of the signal ST wave packet satisfy the non-collinear phase-matchings ($\Delta\theta_s \neq 0$), and Eq. (5b) becomes

$$\omega_i^2 n_i^2 = \omega_p^2 n_p^2 + \omega_s^2 n_s^2 - 2\omega_p n_p \omega_s n_s \cos \Delta\theta_s, \tag{7}$$

where, $\Delta\theta_s$ is the non-collinear angle between the signal and pump, which is also the propagating angle of the frequency $\omega_s = \omega_{s0} + \Omega_s$ with respect to the vertex frequency ω_{s0} within the signal ST wave packet in the x - y - z coordinates. By substituting Eqs. (5a) and (6) into Eq. (7), replacing ω_s by $\omega_{s0} + \Omega_s$, and using the narrowband approximation $\Omega_s^2 \approx 0$, we get the angle-dependent phase-matching spectrum (ST spectrum) of the type-I OPA that is given by Eq. (2) (see equation derivation in Supplementary Note 2 of Supplementary information).

Gain spectrum of OPA and amplified intensity. Under the undepleted pump approximation, the gain G of OPA, as well as the output intensities of the signal,

$I_s(L)$ and idler $I_i(L)$ are given by⁴⁸

$$G = \begin{cases} \frac{\Gamma^2}{\Gamma^2 - (\frac{\Delta k}{2})^2} \sinh^2 \left[L \sqrt{\Gamma^2 - (\frac{\Delta k}{2})^2} \right], & \text{for } \Gamma^2 \geq (\frac{\Delta k}{2})^2 \\ \frac{\Gamma^2}{(\frac{\Delta k}{2})^2 - \Gamma^2} \sin^2 \left[L \sqrt{2\omega_s^2 \omega_i^2 d_{\text{eff}}^2 I_p^2 - \Gamma^2} \right], & \text{for } \Gamma^2 < (\frac{\Delta k}{2})^2 \end{cases} \quad (8a)$$

$$\Gamma^2 = \frac{n_p n_s n_i \epsilon_0 c^3}{n_p n_s n_i \epsilon_0 c^3}, \quad (8b)$$

$$\Delta \mathbf{k} = \mathbf{k}_p - \mathbf{k}_s - \mathbf{k}_i, \quad (8c)$$

$$I_s(L) = I_s(0) \cdot (1 + G), \quad (8d)$$

$$I_i(L) = I_i(0) \frac{\omega_i}{\omega_s} G, \quad (8e)$$

where, L is the crystal length, d_{eff} is the effective nonlinear coefficient, and I_p is the undepleted strong pump intensity.

Propagation of ST wave packet. The angular spectrum method is used to simulate the free propagation of a ST wave packet in vacuum, which from the position $z = 0$ to the position z is governed by

$$E(x, z, t) = 1/2\pi \int E(x, z, \omega) \exp(i\omega t) d\omega, \quad (9a)$$

$$E(x, z, \omega) = 1/2\pi \int A(k_x, z, \omega) \exp(ik_x x) dk_x, \quad (9b)$$

$$A(k_x, z, \omega) = A(k_x, z = 0, \omega) \exp(ikz \sqrt{1 - k_x^2/k^2}), \quad (9c)$$

$$A(k_x, z = 0, \omega) = \int E(x, z = 0, \omega) \exp(-ik_x x) dx, \quad (9d)$$

$$E(x, z = 0, \omega) = \int E(x, z = 0, t) \exp(-i\omega t) dt. \quad (9e)$$

The local-time integral intensity distributions at the position z is given by

$$I(x, z) \propto \int |E(x, z, t)|^2 dt. \quad (10)$$

Data availability

The data that support the findings of this study are available from the corresponding author upon request.

Code availability

The code that supports the findings of this study is available from the corresponding author upon request.

Received: 29 June 2022; Accepted: 11 November 2022;

Published online: 21 November 2022

References

- Wan, C., Cao, Q., Chen, J., Chong, A. & Zhan, Q. Toroidal vortices of light. *Nat. Photonics* **16**, 519–522 (2022).
- Zdagkas, A. et al. Observation of toroidal pulses of light. *Nat. Photonics* **16**, 523–528 (2022).
- Chong, A., Wan, C., Chen, J. & Zhan, Q. Generation of spatiotemporal optical vortices with controllable transverse orbital angular momentum. *Nat. Photonics* **14**, 350–354 (2020).
- Shen, Y., Hou, Y., Papasimakis, N. & Zheludev, N. I. Supertoroidal light pulses as electromagnetic skyrmions propagating in free space. *Nat. Commun.* **12**, 5891 (2021).
- Wong, L. J., Christodoulides, D. N. & Kaminer, I. The complex charge paradigm: A new approach for designing electromagnetic wavepackets. *Adv. Sci.* **7**, 1903377 (2020).
- Wong, L. J. & Kaminer, I. Abruptly Focusing and defocusing needles of light and closed-form electromagnetic wavepackets. *ACS Photonics* **4**, 1131–1137 (2017).
- Wong, L. J. & Kaminer, I. Ultrashort tilted-pulse-front pulses and nonparaxial tilted-phase-Front beams. *ACS Photonics* **4**, 2257–2264 (2017).
- Porrás, M. A. Gaussian beams diffracting in time. *Opt. Lett.* **42**, 4679–4682 (2017).
- Efremidis, N. K. Spatiotemporal diffraction-free pulsed beams in free-space of the Airy and Bessel type. *Opt. Lett.* **42**, 5038–5041 (2017).
- Parker, K. J. & Alonso, M. A. Longitudinal iso-phase condition and needle pulses. *Opt. Express* **24**, 28669–28677 (2016).
- Sainte-Marie, A., Gobert, O. & Quére, F. Controlling the velocity of ultrashortlight pulses in vacuum through spatio-temporal couplings. *Optica* **4**, 1298–1304 (2017).
- Froula, D. H. et al. Spatiotemporal control of laser intensity. *Nat. Photonics* **12**, 262–265 (2018).
- Kondakci, H. E. & Abouraddy, A. F. Diffraction-free pulsed optical beams via space-time correlations. *Opt. Express* **24**, 28659–28668 (2016).
- Kondakci, H. E. & Abouraddy, A. F. Diffraction-free space-time light sheets. *Nat. Photonics* **11**, 733 (2017).
- Shen, Y. & Rosales-Guzmán, C. Nonseparable states of light: from quantum to classical. *Laser Photonics Rev.* **16**, 2100533 (2022).
- Palastro, J. P. et al. Dephasingless laser wakefield acceleration. *Phys. Rev. Lett.* **124**, 134802 (2020).
- Turnbull, D. et al. Ionization waves of arbitrary velocity. *Phys. Rev. Lett.* **120**, 225001 (2018).
- Bhaduri, B., Yessenov, M. & Abouraddy, A. F. Space-time wave packets that travel in optical materials at the speed of light in vacuum. *Optica* **6**, 139–146 (2019).
- Kondakci, H. E. & Abouraddy, A. F. Optical space-time wave packets having arbitrary group velocities in free space. *Nat. Commun.* **10**, 929 (2019).
- Hall, L. A., Yessenov, M. & Abouraddy, A. F. Arbitrarily accelerating space-time wave packets. *Opt. Lett.* **47**, 694–697 (2022).
- Yessenov, M. & Abouraddy, A. F. Accelerating and decelerating space-time optical wave packets in free space. *Phys. Rev. Lett.* **125**, 233901 (2020).
- Bhaduri, B. et al. Broadband space-time wave packets propagating 70 m. *Opt. Lett.* **44**, 2073–2076 (2019).
- Yessenov, M., Hall, L. A. & Abouraddy, A. F. Engineering the optical vacuum: Arbitrary magnitude, sign, and order of dispersion in free space using space-time wave packets. *ACS Photonics* **8**, 2274–2284 (2021).
- Hall, L. A. & Abouraddy, A. F. Free-space group-velocity dispersion induced in space-time wave packets by V-shaped spectra. *Phys. Rev. A* **104**, 013505 (2021).
- Bhaduri, B., Yessenov, M. & Abouraddy, A. F. Anomalous refraction of optical spacetime wave packets. *Nat. Photonics* **14**, 416–421 (2020).
- Hall, L. A., Yessenov, M. & Abouraddy, A. F. Space-time wave packets violate the universal relationship between angular dispersion and pulse-front tilt. *Opt. Lett.* **46**, 1672–1675 (2021).
- Yessenov, M., Hall, L. A., Ponomarenko, S. A. & Abouraddy, A. F. Veiled Talbot effect. *Phys. Rev. Lett.* **125**, 243901 (2020).
- Kondakci, H. E. & Abouraddy, A. F. Airy wave packets accelerating in space-time. *Phys. Rev. Lett.* **120**, 163901 (2018).
- Saari, P. & Reivelt, K. Generation and classification of localized waves by Lorentz transformations in Fourier space. *Phys. Rev. E* **69**, 036612 (2004).
- Porrás, M. A. Nature, diffraction-free propagation via space-time correlations, and nonlinear generation of time-diffracting light beams. *Phys. Rev. A* **97**, 063803 (2018).
- Yessenov, M., Bhaduri, B., Kondakci, H. E. & Abouraddy, A. F. Classification of propagation-invariant space-time wave packets in free space: Theory and experiments. *Phys. Rev. A* **99**, 023856 (2019).
- Kondakci, H. E. et al. Synthesizing broadband propagation-invariant space-time wave packets using transmissive phase plates. *Opt. Express* **26**, 13628–13638 (2018).
- Park, J., Kang, J. H., Kim, S. J., Liu, X. & Brongersma, M. L. Dynamic reflection phase and polarization control in metasurfaces. *Nano Lett.* **17**, 407–413 (2017).
- Zhang, L. et al. Space-time-coding digital metasurfaces. *Nat. Commun.* **9**, 4334 (2018).
- Shaltout, A. M. et al. Spatiotemporal light control with frequency-gradient metasurfaces. *Science* **365**, 374 (2019).
- Ogino, J. et al. 10 J operation of a conductive-cooled Yb:YAG active-mirror amplifier and prospects for 100 Hz operation. *Opt. Lett.* **46**, 621–624 (2021).
- Yu, L. et al. High-contrast front end based on cascaded XPWG and femtosecond OPA for 10-PW-level Ti:sapphire laser. *Opt. Express* **26**, 2625–2633 (2018).
- Musgrave, I. et al. Picosecond optical parametric chirped pulse amplifier as a preamplifier to generate high-energy seed pulses for contrast enhancement. *Appl. Opt.* **49**, 6558–6562 (2010).
- Orlov, S., Piskarskas, A. & Stabinis, A. Focus wave modes in optical parametric generators. *Opt. Lett.* **27**, 2103–2105 (2002).

40. Butkus, R., Orlov, S., Piskarskas, A., Smilgevičius, V. & Stabinis, A. Phase matching of optical X-waves in nonlinear crystals. *Opt. Commun.* **244**, 411–421 (2005).
41. Orlov, S., Stabinis, A., Smilgevičius, V., Valiulis, G. & Piskarskas, A. Parametric excitation of X-waves by downconversion of Bessel beams in nonlinear crystals. *Opt. Lett.* **32**, 68–70 (2007).
42. Dubietis, A., Smilgevičius, V., Stabinis, A., Valiulis, G. & Piskarskas, A. Optical parametric amplification of X-shaped localised wave-packets. *Quantum Electron.* **39**, 599–608 (2009).
43. Jedrkiewicz, O., Clerici, M., Rubino, E. & Trapani, P. D. Generation and control of phase-locked conical wave packets in type-I seeded optical parametric amplification. *Phys. Rev. A* **80**, 033813 (2009).
44. Gui, G., Brooks, N. J., Kapteyn, H. C., Murnane, M. M. & Liao, Ch-T. Second-harmonic generation and the conservation of spatiotemporal orbital angular momentum of light. *Nat. Photonics* **15**, 608–613 (2021).
45. Hancock, S. W., Zahedpour, S. & Milchberg, H. M. Second-harmonic generation of spatiotemporal optical vortices and conservation of orbital angular momentum. *Optica* **8**, 594–597 (2021).
46. Wu, H.-J. et al. Conformal frequency conversion for arbitrary vectorial structured light. *Optica* **9**, 187–196 (2022).
47. Hall, L. A. & Abouraddy, A. F. Spectral reorganization of space-time wave packets in presence of normal group-velocity dispersion. Preprint at <https://arxiv.org/abs/2206.05387> (2022).
48. Schimpf, D. N., Rothhardt, J., Limpert, J., Tünnermann, A. & Hanna, D. C. Theoretical analysis of the gain bandwidth for noncollinear parametric amplification of ultrafast pulses. *J. Opt. Soc. Am. B* **24**, 2837–2846 (2007).

Acknowledgements

This work was supported by Zhangjiang Laboratory. Open Access funding enabled and organized by Zhangjiang Laboratory.

Author contributions

Z.L. developed the concept, derived the equations, carried out the simulation, and prepared the manuscript. Y.L. and R.L. optimized the concept, revised the manuscript, and discussed the application. All authors discussed the results and commented on the manuscript.

Competing interests

The authors declare no competing interests.

Additional information

Supplementary information The online version contains supplementary material available at <https://doi.org/10.1038/s42005-022-01085-w>.

Correspondence and requests for materials should be addressed to Zhaoyang Li.

Peer review information *Communications Physics* thanks the anonymous reviewers for their contribution to the peer review of this work. Peer reviewer reports are available.

Reprints and permission information is available at <http://www.nature.com/reprints>

Publisher's note Springer Nature remains neutral with regard to jurisdictional claims in published maps and institutional affiliations.



Open Access This article is licensed under a Creative Commons Attribution 4.0 International License, which permits use, sharing, adaptation, distribution and reproduction in any medium or format, as long as you give appropriate credit to the original author(s) and the source, provide a link to the Creative Commons license, and indicate if changes were made. The images or other third party material in this article are included in the article's Creative Commons license, unless indicated otherwise in a credit line to the material. If material is not included in the article's Creative Commons license and your intended use is not permitted by statutory regulation or exceeds the permitted use, you will need to obtain permission directly from the copyright holder. To view a copy of this license, visit <http://creativecommons.org/licenses/by/4.0/>.

© The Author(s) 2022